New insights into Kawah Ijen's volcanic system from the wet volcano workshop experiment

HENDRA GUNAWAN[1], CORENTIN CAUDRON[2,3,4]*, JOHN PALLISTER[5], SOFYAN PRIMULYANA[1], BRUCE CHRISTENSON[6], WENDY MCCAUSLAND[5], VINCENT VAN HINSBERG[7], JENNIFER LEWICKI[8], DMITRI ROUWET[9], PETER KELLY[5], CHRISTOPH KERN[5], CYNTHIA WERNER[10], JEFFREY B. JOHNSON[11], SRI BUDI UTAMI[7], DEVY KAMIL SYAHBANA[1], UGAN SAING[1], SUPARJAN[1], BAMBANG HERI PURWANTO[1], CHRISTINE SEALING[2], MARIA MARTINEZ CRUZ[12], SUKIR MARYANTO[13], PHILIPSON BANI[14], ANTOINE LAURIN[14], AGATHE SCHMID[2], KYLE BRADLEY[2], I GUSTI MADE AGUNG NANDAKA[1] & MOCHAMMAD HENDRASTO[1]

[1]*Centre for Volcanology and Geological Hazard Mitigation, Geological Agency, Ministry of Energy and Mineral Resources, Jalan Diponegoro 57, Bandung 40122, Indonesia*

[2]*Earth Observatory of Singapore, Nanyang Technological University, 50 Nanyang Avenue, Block N2-01a-15, Singapore 639798*

[3]*Royal Observatory of Belgium, Seismology Section, 1180 Uccle, Belgium*

[4]*Department of Earth and Environmental Sciences, Université Libre de Bruxelles, 1050 Bruxelles, Belgium*

[5]*US Geological Survey, Cascades Volcano Observatory, 1300 SE Cardinal Ct 100, Vancouver, Washington 98683, USA*

[6]*National Isotope Centre, GNS Science, PB 31-312, Lower Hutt, New Zealand*

[7]*Department of Earth and Planetary Sciences, McGill, 3450 University St, Montreal, Quebec H3A 2A7, Canada*

[8]*US Geological Survey, 345 Middlefield Rd, MS 434, Menlo Park, CA 95025, USA*

[9]*Istituto Nazionale di Geofisica e Vulcanologia, Sezione di Bologna, Via Donato Creti 12, 40128 Bologna, Italy*

[10]*Alaska Volcano Observatory – Volcano Emissions Project, 4230 University Drive, Anchorage AK 99508, USA*

[11]*Department of Geosciences, Boise State University, 1910 University Ave, Boise, ID 83725, USA*

[12]*Observatorio Vulcanologico y Sismologico de Costa Rica, 2346-3000 Heredia, Costa Rica*

[13]*Department of Physics, Universitas Brawijaya, Malang, Jawa Timur 65145, Indonesia*

[14]*Laboratoire Magmas et Volcans, University Blaise Pascal – CNRS – IRD, OPGC, 63000, Clermont-Ferrand, France*

**Corresponding author (e-mail: corentin.caudron@gmail.com)*

Abstract: Volcanoes with crater lakes and/or extensive hydrothermal systems pose significant challenges with respect to monitoring and forecasting eruptions, but they also provide new opportunities to enhance our understanding of magmatic–hydrothermal processes. Their lakes and hydrothermal systems serve as reservoirs for magmatic heat and fluid emissions, filtering and delaying the surface expressions of magmatic unrest and eruption, yet they also enable sampling and monitoring of geochemical tracers. Here, we describe the outcomes of a highly focused international experimental campaign and workshop carried out at Kawah Ijen volcano, Indonesia, in September 2014, designed to answer fundamental questions about how to improve monitoring and eruption forecasting at wet volcanoes.

From: OHBA, T., CAPACCIONI, B. & CAUDRON, C. (eds) *Geochemistry and Geophysics of Active Volcanic Lakes*. Geological Society, London, Special Publications, **437**, http://doi.org/10.1144/SP437.7

Volcanoes hosting crater lakes and/or extensive hydrothermal systems represent an important volcanic subclass, which we will refer to here as 'wet volcanoes'. This subclass of volcanoes is characterized by specific hazards (mudflows, lahars, cid effluent) and monitoring challenges, as well as research monitoring opportunities (Rouwet *et al.* 2014*a*, *b*; Manville 2015). Ruapehu in New Zealand and Kawah Ijen volcano in East Java, Indonesia, can be regarded as 'type localities' for such systems, with both hosting large active crater lakes and dynamic volcanic–hydrothermal systems. Whereas the Ruapehu system is increasingly well understood (Nairn *et al.* 1979; Christenson *et al.* 2010; Jolly *et al.* 2010; Kilgour *et al.* 2014), precursors to eruptions remain difficult to identify, emphasizing the need to improve recognition of very subtle changes in these magmatic systems, which will lead to more accurate hazard monitoring.

A volcanic crisis at Kawah Ijen in 2011–12 (Caudron *et al.* 2015*a*, *b*), raised concerns within the Center for Volcanology and Geologic Hazard Mitigation of Indonesia's Geological Agency (CVGHM-GA) that even with their existing monitoring networks, the understanding of Kawah Ijen and other wet volcanoes is insufficient to adequately assess the hazards and mitigate the risks posed by future phreatic or phreato-magmatic eruptions. An international workshop took place from 14–21 September 2014 at Kawah Ijen volcano to conduct monitoring experiments for potential use at wet volcanoes in Indonesia, and elsewhere.

Participants (25 from 10 countries) brought a variety of geophysical and geochemical instruments to the volcano for campaign measurements to test techniques and evaluate their feasibility for the long-term CVGHM monitoring programme (Gunawan *et al.* 2014). The monitoring experiments utilized broadband seismic and infrasound arrays, thermal infrared imaging of surface temperatures, differential optical absorption spectroscopy (DOAS) for SO_2 emission rate measurement, ultraviolet SO_2 cameras, a multiple gas analyser system (multi-GAS) for real-time measurement of multiple plume gas species, newly developed diode-laser spectroscopy for atmospheric CO_2 concentration measurement, and sampling of fumaroles and water for geochemical analyses. Additionally, gypsum associated with the 1817 eruption of Kawah Ijen was sampled and analysed to compare the pre-1817 lake composition to that of today (Utami 2015).

This article will first briefly describe the volcanic settings, the monitoring system and the volcanic activities during the workshop. For each technique, we briefly describe the methodology directly followed by the main results and analyses. We then propose new interpretations of the magmatic and hydrothermal processes together with the primary outcome of this workshop: the identification of Ruapehu volcano, New Zealand, as a 'sister volcano' of Kawah Ijen, with remarkably similar and well-studied geological structures and geochemical/geophysical processes that can therefore act as a model to understand Kawah Ijen and interpret its signals. Finally, recommendations relevant to the Kawah Ijen volcano and 'wet volcanoes', in general, are proposed.

Volcanic settings, activity and general monitoring network

Kawah Ijen is an active volcano in East Java (Fig. 1a, b), Indonesia, located along the structural margin of the 20 km-diameter Kawah Ijen caldera (Handley *et al.* 2007; Van Hinsberg *et al.* 2010*a*). It hosts the largest natural hyper-acidic crater lake in the world (30 Mm^3 with pH <1), has a high-temperature fumarole field (maximum 450°C measured *in situ* during this investigation) located on a silicic magmatic dome adjacent to the lake, and has a history of frequent small phreatic emissions and infrequent but much larger phreato-magmatic eruptions (Takano *et al.* 2004; Caudron *et al.* 2015*a*). The last major eruption in 1817 expelled large volumes of acidic lake water, producing lahars that inundated now highly populated areas (Bosch 1858; Caudron *et al.* 2015*a*). Kawah Ijen continuously drains hydrothermal acidic water with high concentrations of fluoride, aluminum and heavy metals into an important agricultural area, resulting in human health hazards (Löhr *et al.* 2005). Further increasing the hazards and risks, dozens of miners each carry up to 90 kg of sulphur per trip out of the fumarole field to the crater rim and then 3 km down the volcano and hundreds of tourists daily visit the crater during amenable weather.

The volcanic crisis at Kawah Ijen in 2011–12 was characterized by swarms of locally felt, distal volcano-tectonic (VT) earthquakes followed by increases in the occurrence of proximal VTs, low-frequency (LF) earthquakes, and intense tremor, as well as a 12°C increase in lake temperature (Caudron *et al.* 2015*b*). In response to a request from the CVGHM-GA, the Volcano Disaster Assistance Program (VDAP) and the Royal Observatory of Belgium (ROB) assisted CVGHM-GA scientists and technicians to improve their seismic network and interpret the unrest.

Since 2010–11 (Caudron *et al.* 2015*a*), the seismic monitoring of Kawah Ijen by CVGHM-GA consists of a network of 8 seismometers telemetered in real-time to an observatory located near the volcano (POS, Fig. 1c). During periods of time when access to the crater is not prohibited due to unrest, the observers from the Kawah Ijen observatory

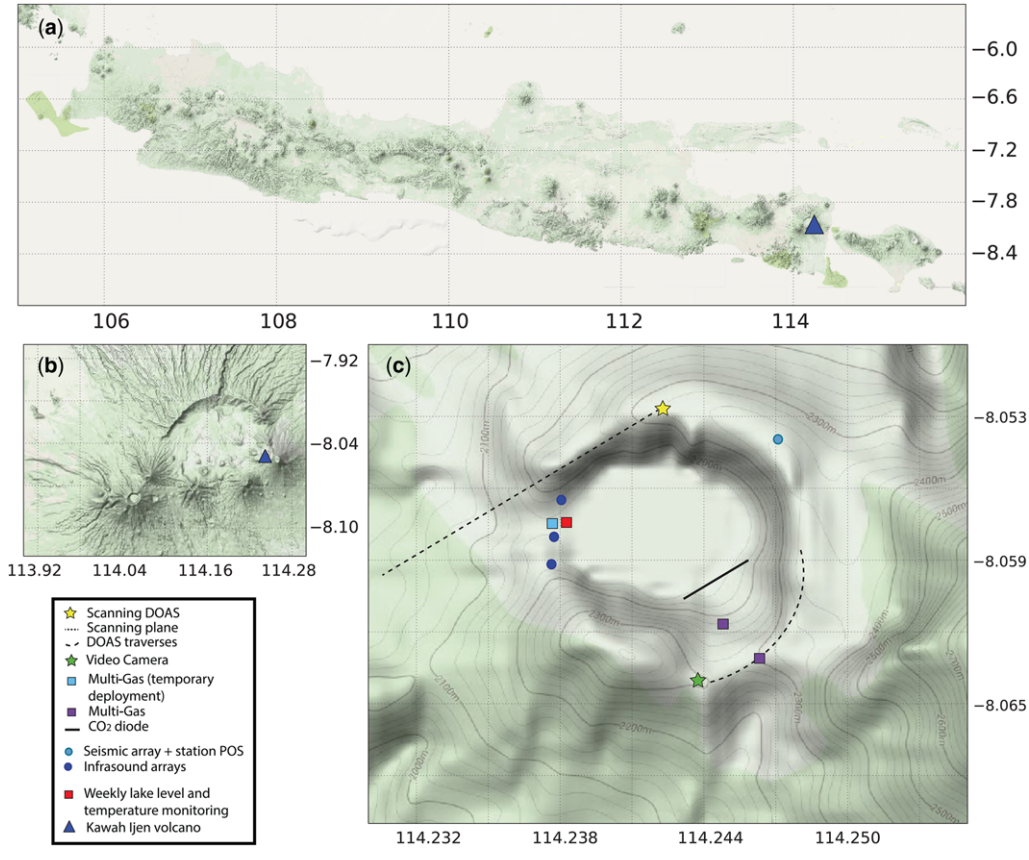

Fig. 1. Location (axes, in decimal degrees) of the different monitoring methods during the workshop: (**a**) Java island with Kawah Ijen location (blue triangle); (**b**) Kawah Ijen caldera; (**c**) Kawah Ijen volcano. The different methods are described in the legend and their respective locations in panel c.

measure the lake temperature every week at a depth of <1 m at the dam (Fig. 1c) using a hand-held thermocouple. The lake level is recorded weekly using a graduated wooden level-rod also located at the dam (Fig. 1c). Since 2010, the lake temperature at the dam is also recorded hourly using an iButton thermochron sensor installed at a depth of *c.* 5 m. The lake is monitored visually during daylight hours by telemetered closed-circuit television (CCTV). Changes in colour or lake activity and rockfalls can be seen when the view is clear. Visual observations are made by observers and sulphur miners regarding changes within the crater. CCTV, lake temperature, and seismic data are viewed, characterized, analysed and archived at the observatory.

Water chemistry data for the Kawah Ijen lake and Banyu Pahit River are available from the early twentieth century (Caudron *et al.* 2015*a*), initially as sporadic measurements, but from 1996 onward at more regular intervals (at least once a year, e.g. Delmelle *et al.* (2000), Takano *et al.* (2004), Van Hinsberg *et al.* (2010*b*)). In addition, a density measurement and chemical analysis were taken in 1805 and 1850, respectively (van Hinsberg *et al.* 2015). The long-term record shows a gradual increase in dissolved element content over time following the lake expulsion in 1817 with present density at the same level as that prior to the 1817 eruption. This suggests a model where the lake reappeared after 1817 as a dilute rain and groundwater-fed reservoir. This reservoir was acidified by the input of volcanic gases and obtained its cation content from leaching of its magmatic host rocks (basalt to dacite, van Hinsberg *et al.* (2015)) as well as material falling in during landslides. On shorter, annual time-scales, lake surface waters reflect dilution by rain in the wet season. Lake water chemistry from 1994 to 2010, sampled and analysed by a variety of groups (Delmelle & Bernard 1994; Delmelle *et al.* 2000; Takano *et al.* 2004; Van Hinsberg

et al. 2010*b*), showed no significant change in composition when seasonal variations were removed. During the 2011–12 crisis, water samples were collected monthly and analysed for anions by ion chromatography (ICion) and cations by atomic absorption (AA) by CVGHM, but the data are ambiguous and more work is needed to assess the compositions that were obtained.

Gas chemistry data are available since the 1990s from direct sampling using Giggenbach-style bottles as conducted by CVGHM and a number of research groups. Unfortunately, these data are for gases sampled at the exits of metal and ceramic pipes used in sulphur mining, and represent a modified gas composition, 200°C cooler than the vents on the top of the dome. In 2008, high-temperature vents were directly sampled and compositions were indeed different (van Hinsberg *et al.* 2015). As such, the presently available dataset of gas compositions cannot provide much information on whether and how compositions have changed over time.

During the workshop, and since at least the end of August 2014, seismicity at Kawah Ijen was low and consisted of low-amplitude, low-frequency tremor (<5 Hz dominant frequency), periodic shallow LF VT earthquakes, deep VT earthquakes, tornillos, rockfalls and emission events. Such seismicity corresponds to the background activity at Kawah Ijen (Caudron *et al.* 2015*a*) and indicates the continuous movement of magmatic gases through the fumarole field and into the bottom of the lake. Regional and teleseismic earthquakes were also recorded but are not relevant to the current activity. Real-time Seismic Amplitude Monitoring (RSAM, Endo & Murray (1991)) values were low and showed low-level variations with the occurrence of tremor as well as the local, regional and teleseismic earthquakes. The lake had its normal blue–green colour with small and subtle areas of upwelling, bubbling evident at the edges of the lake and events of visible evaporation across the lake surface.

The last significant increase in activity was on 6–7 May 2014, when there was increased upwelling and bubbling in the lake coincident with an increase in tremor.

Methodologies, results and discussion during the workshop

Seismic and infrasound arrays

Seismic array. The characteristic seismicity recorded at Kawah Ijen volcano was described by Caudron *et al.* (2015*a*, *b*). The objective of the seismic array was to better constrain the origin of the continuous seismic tremor that has yet to be properly characterized. Two arrays of 5 broadband sensors (Guralp 6TD, 30 s of lower natural frequency, 100 Hz of sampling frequency) of different apertures (80 m for two and a half days and 25 m for less than a day) were installed on the northern crater rim (Fig. 1c). However, no clear period of tremor was recorded during the experiment. We therefore focused this study on the comparison with other parameters such as the Multi-GAS.

Infrasound array. Three infrasound arrays of 3, 3 and 2 sensors were deployed at the west end of the lake for a four-day interval (Fig. 2). Sensors were located close to the lakeshore in an attempt to identify possible lake distension events (e.g. bubble collapse). Although no infrasound activity was identified on the lake surface during the deployment interval, a stationary and continuous tremor was observed when ambient wind was low. In addition, episodic crater-wall rockfalls occurring approximately 10 times per day were detected and were characterized as transient low-amplitude moving sources. The rockfalls are incidental and their signals are not focused upon here, but their signal character is similar to rockfall events described by Johnson & Ronan (2015).

The continuous low-amplitude tremor is particularly interesting in that it possesses a relatively high spectral content of 8–15 Hz (Fig. 3) compared to other volcanic tremors associated with magmatic sources (e.g. Johnson & Ripepe 2011). The tremor appears to locate coincidentally with vigorous fumarolic activity located at the sulphur mines at the SE edge of the lake (Fig. 2), approximately 1 km distant and directly within line-of-sight.

Inferred source locations in Figure 2 correspond to contours of equal semblance (e.g. Ripepe *et al.* (2007), Jones & Johnson 2011) using data recorded at arrays E and M. The presumed fumarole source is intermittently detected owing to high levels of ambient wind. When wind is high, typically during local daytime, the peak cross-correlation signal amplitude drops (Fig. 4a) and the corresponding recorded power increases (Fig. 4c). This power is calculated in hour-long averages as the pressure amplitude squared divided by the atmospheric impedance. During low wind conditions, robust correlation lag times are determined for inter-array (E v. M) and intra-array channel comparisons.

Phase delays of 81 samples between arrays M and E provide constraints on the tremor source. A circular search region in Figure 2 is examined for candidate sources that are fixed to the lake and Aster GDEM surface. Expected delay times are calculated across a grid space and compared with the stationary cross-correlation lag time of 0.2025 s (81 samples). Absolute differences between lag time

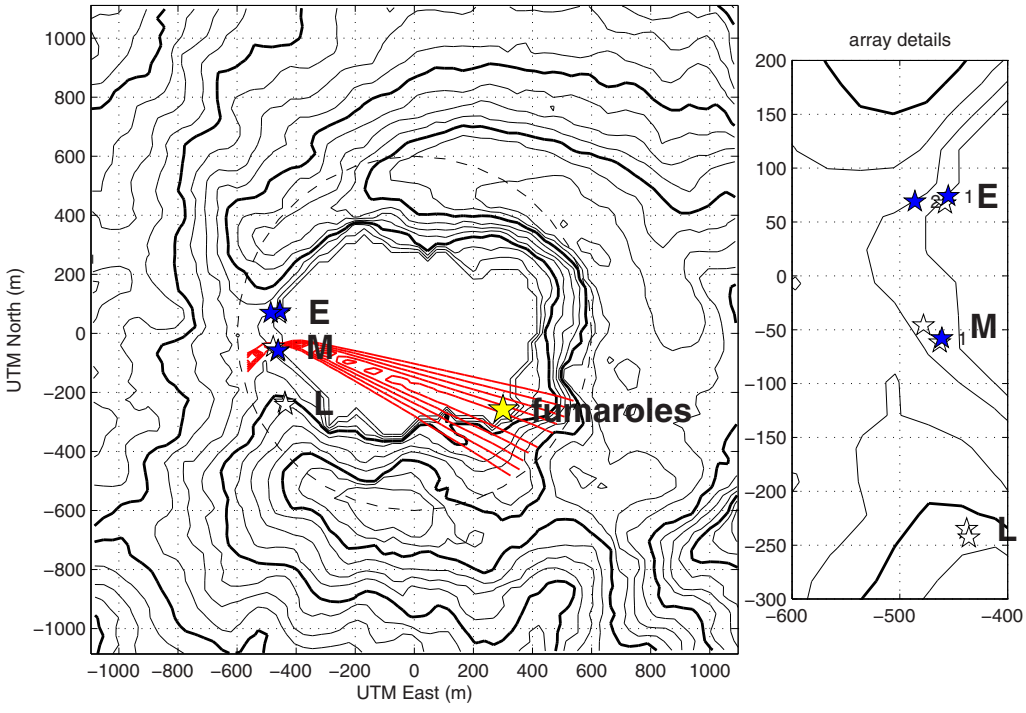

Fig. 2. Locations of infrasound arrays and inferred tremor source: Characteristic delay time of 81 samples between arrays M and E indicates a source of the continuous tremor located in a ESE direction from the west end of the lake. Residual errors of 0.01, 0.02, 0.03, 0.04, 0.05 s for sources fixed to the DEM surface are drawn as contours. Lowest residual contour (0.01 s) intersects with the known location of active fumarolic activity.

and predicted phase delay are plotted as contours with 0.01 s intervals.

The short infrasound deployment at Kawah Ijen identified a source of tremor that was likely continuous during the four-day observation period. Continuous infrasound monitoring of this tremor would be useful in order to identify potential changes in the quality, amplitude or spectral nature of this source. Such changes might presage or suggest other changes in the Kawah Ijen system.

Closer comparison between infrasound and seismic radiation, which is common in other volcano studies (e.g. Arrowsmith *et al.* 2010), should also be illuminating. In particular if lake degassing and/or explosions in the lake become more vigorous there should be a detectable seismo-acoustic source.

A shortcoming of the September 2014 deployment is the high level of noise relative to signal for the study interval. Wind at the west end of the lake was particularly strong and the fumarole signal recorded was typically less than 0.1 Pa peak-to-peak. Careful selection of low-noise, low-wind deployment sites will be critical for future work and arrays of more than 3 sensors will help to distinguish signal from noise. If the fumarole field is to be targeted specifically for monitoring, a dedicated array of two or more infrasound sensors could be adequately deployed as close as 100 m from this locale.

Thermal monitoring

In situ *temperature measurements.* Kawah Ijen lake water and fumarole vent temperatures were monitored by a thermocouple to determine temperature variability and assess the potential of point temperature measurements in monitoring efforts. Air temperature and air humidity were simultaneously logged to determine the effect of atmospheric conditions on lake and fumarole temperatures.

Temperatures were measured using a type-K thermocouple directly connected to a battery-powered single-channel datalogger that stored the temperature every 30 seconds. The accuracy of this method is $\pm 1^{\circ}$C with a precision of $\pm 0.2^{\circ}$C. The fumarole thermocouple wires had ceramic insulation and a 1 m long quartz-glass sleeve sealed at the end to withstand the chemically aggressive and hot vent environment (vent area C; Fig. 5). Away

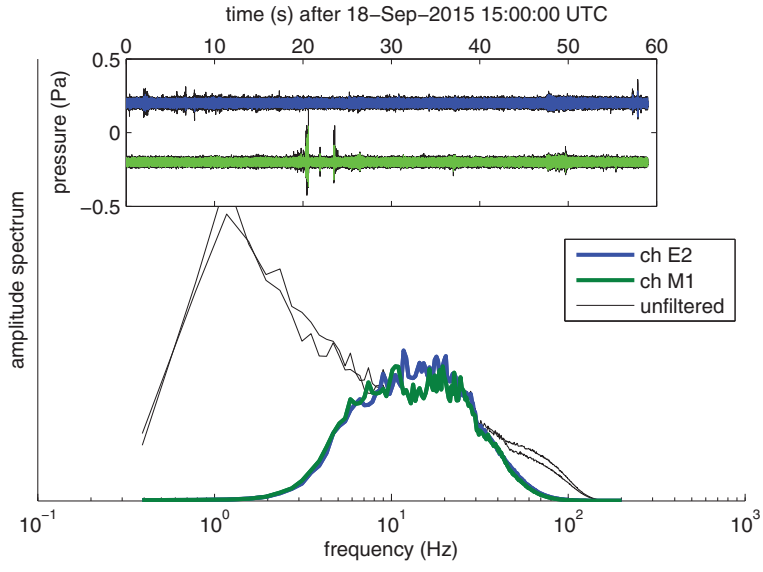

Fig. 3. Infrasound example record and spectrum. Amplitude periodograms for 1–100 Hz and filtered (0.5–100 Hz) data respectively. Black thin line is broadband (0.5–100 Hz) record and blue/green (darker/lighter) thicker lines are 5–50 Hz filtered traces. Example shown corresponds to the highest inter-channel cross-correlation values for 4-day study interval (see Fig. 4). Inset: hour-long infrasound record from channel 2 of E Array and 1 of M array starting 18 September at 15:00:00 UTC (22:00:00 local time).

from the vent, the ceramic insulated wire was supported on bamboo poles and the logger was placed on a relatively cold part of the dome. The glass tube was inserted about 20 cm into grey, fractured rock without any precipitates just below a flaming fumarole, which represents the highest-temperature fumarole type (van Hinsberg *et al.* 2015). These flaming fumaroles result from oxidation of sulphur species upon contact with the air and produce the 'blue flames' that Kawah Ijen is rapidly becoming known for. This exothermic oxidation can result in surface gas temperatures that exceed those measured in deep fissures in the dome. The lake thermocouple had teflon insulation and was placed in end-sealed teflon tubing to protect it from the corrosive water. A bamboo pole was used to position it at *c.* 1.5 m depth in the lake with the teflon-coated wire leading to the logger, which was hidden *c.* 1 m above the lake level (approximate location in Fig. 5b). The air temperature and humidity were recorded every minute using an Omega battery-operated logger attached to a 2 m-long bamboo pole that was placed at the site of the lake water logger, approximately 5 m above the lake level.

Temperature and humidity logs for the seven-day measurement period (16–23 September) are shown in Figure 6. The 0.5°C difference between hourly recorded iButton temperatures (thermochron sensor installed at a depth of *c.* 5 m, see above) and thermocouple values is well within the accuracy of the thermocouple. Air temperature follows the diurnal cycle, with a 10°C difference between day and night. Humidity also shows diurnal variations, but the signal is less regular. In general, humidity is higher at night. The rapid variations in humidity, especially on 20 September, probably reflect the plume wafting over the logger. Lake water temperature is essentially constant at 33.0 ± 0.5°C. However, a small, approximately 1°C diurnal variation is present with statistically significant higher temperatures during the day. Lake water tracks air temperature, with the highest values on the 18 September.

Fumarole vent temperatures vary from 330°C to 355°C. There is periodicity in the signal, which tracks the diurnal variations in air temperature, albeit with a 2.5-hour lag. However, there are marked deviations from this periodicity, such as the high temperatures in the early morning of 17 September.

The protective measures for the thermocouples were mostly successful for the full duration of measurement (7 days). The air logger was covered by native sulphur needles on the side facing the fumaroles, but was clear on the other side and no adverse effect of this coating was seen in the measurements. The thermocouple in the fumarole vent was completely unharmed, but the ceramic insulation on the

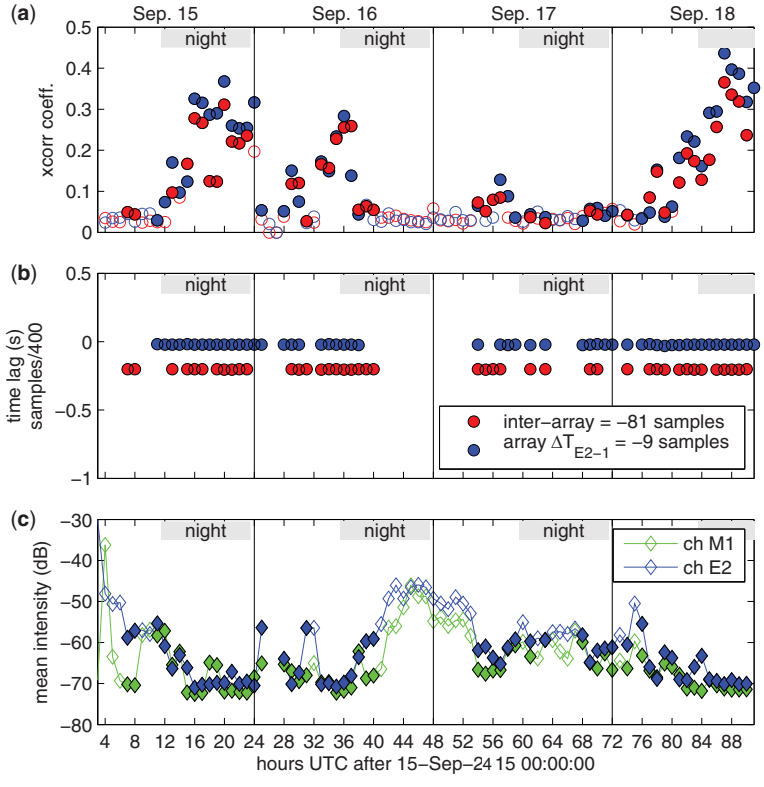

Fig. 4. Four-day sequence of infrasound tremor detections. (**a**) Normalized cross-correlation coefficient calculated for hour-long windows of data filtered between 5 and 50 Hz. Blue (darker) symbols correspond to comparison of channels 1 and 2 of array E and red (lighter) symbols correspond to channels 1 of array M with channel 2 of array M. Filled circles correspond to cross correlation windows with phase lags of ~9 samples and ~81 samples for intra- and inter-array comparisons respectively. (**b**) Chronology of cross-correlation phase lags for intra-array (blue/darker) and inter-array (red/lighter) hour-long data windows. (**c**) Average acoustic power intensity (in dB) for hour-long windows. Intensity is quantified as the log of power per unit area, i.e. 10 × log10 (W m^{-2}). Periods of local night-time (11:30–23:30 UTC) are indicated by grey shading.

wire leading away from it had peeled away where it was connected to the bamboo poles, probably because of wind moving the wire. This led to electrical connectivity issues, which makes the signal beyond the night of 19 September difficult to interpret. For a long-term deployment, we recommend extending the glass sleeve to cover the full length over which high temperatures are encountered, and coating the wires in teflon for the remainder.

Temperature variations mainly reflect diurnal periodicity, with an amplitude of 10°C in air temperature, 1°C in lake water temperature at 1.5 m depth, and 15–20°C in fumarole vent temperature. The limited variability in lake water temperature is in agreement with surface forcing by diurnal air temperature changes, and suggests a constant lake water temperature at depth. For volcanic monitoring purposes, a temperature sensor should thus be installed at greater than 1.5 m depth.

The correlation between fumarole vent temperature and air temperature indicates that the vents respond to changes in air temperature. This could result from air entering the dome at its base in a chimney effect, or lowering of dome-rock temperature to that of ambient air. The 2.5-hour lag time and the larger amplitude of fumarole temperature variations argue against an air inflow model, as a more rapid response would be expected in this case as well as a diurnal temperature amplitude equal to that of the outside air, unless the mixing ratio changed at the same time. We therefore prefer the alternative explanation, where the lag in response results from the low thermal conductivity of the vent host rocks. At night, the plume generally rises straight out of the crater, whereas it often hugs the dome during the day, which would further promote loss of heat from the rocks at night. This interpretation does mean that our thermocouple

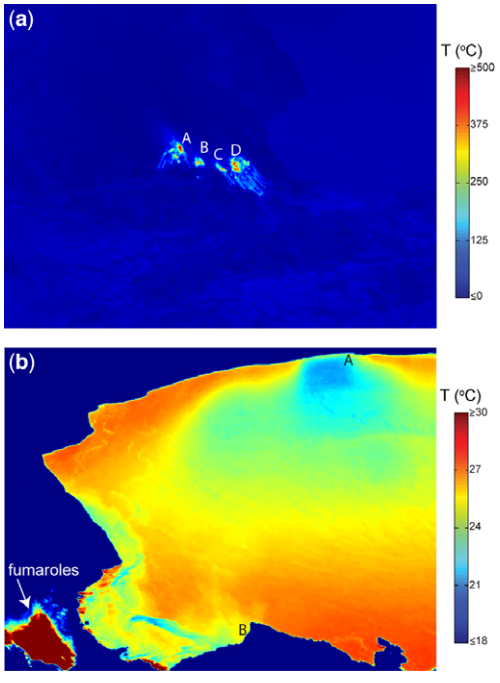

Fig. 5. (**a**) Thermal image of the dome fumarole field taken from the southeastern crater rim on 15 September 2014. Vent areas A–D are shown. (**b**) Thermal image of the crater lake taken from the southeastern crater rim on 18 September 2014. Approximate locations of *in situ* thermochron iButton thermal sensor at *c.* 5 m depth and thermocouple at 2 m depth are labelled A and B, respectively.

measured rock temperature rather than gas temperature, because the high gas flow of this fumarole prohibits temperature equilibration at the vent. As such, the thermocouple could not have recorded any short-duration temperature fluctuations. Deviations from the diurnal periodicity are also observed, indicating that additional processes affect vent temperature, such as gas flow-rate or changes in air–gas mixing ratio. In terms of their applicability to monitoring, these results indicate that changes in volcanic activity need to be accompanied by a more than a 25°C change in vent temperature to be reliably detected. Moreover, continuous recording rather than punctuated campaign measurement is recommended to conclusively assign a change in temperature to increased (or decreased) activity.

In conclusion, thermocouples provide a low-cost monitoring tool that is simple to install and simple to maintain at Kawah Ijen, if properly protected against the harsh environment. However, the method requires manual retrieval of data unless a telemetered logger is used.

Thermal infrared. A forward-looking infrared (FLIR) model T650sc thermal imaging camera was used on the crater rim of Kawah Ijen to image the surface apparent (radiant) temperatures of the dome fumarole field and the crater lake. The FLIR T650sc uses an uncooled microbolometer as its thermal sensor, which measures infrared radiation emitted by surface features in the 8–14 μm spectral range. The camera has measurement sensitivity and accuracy at around 30°C of $\pm$0.02 and 1°C, respectively, and thermal infrared (TIR) image resolution of 640 × 480 pixels. The image acquisition rate can be set up to 30 Hz. A 25° lens was used. The camera's measurement range was set to 100–650°C and −40–150°C for imaging of the dome fumarole field and lake, respectively. Thermal imaging of the high-temperature fumarole field was conducted on 15 September 2014 at *c.* 12:00–12:30 p.m. To minimize the influence of solar heating and reflection on the relatively low-temperature lake surface, thermal images of the lake surface were acquired during the pre-dawn period of 3:30–4:00 a.m. on 18 September 2014. The camera performs internal emissivity and atmospheric corrections based on user inputs of emissivity, path length, ambient temperature and relative humidity, and reflected ambient temperature. Ambient temperature and relative humidity were measured during TIR image acquisition using an Omega RH 820 temperature/humidity sensor. An emissivity of 0.96 was used. To minimize absorption effects of steam, volcanic gas (e.g. SO_2) and aerosols on the TIR image quality, images were selected when the wind was from a northerly direction (i.e. when the volcanic plume was positioned over the southern crater rim, rather than over the lake).

TIR images of the dome fumarole field and the central to western part of the crater lake are shown in Figure 5b. Four main areas of vents are labelled (A–D) in Figure 5a. The highest apparent temperature (512°C) was observed within area A, whereas maximum apparent temperatures observed within areas B, C, and D were 387°C, 382°C and 466°C, respectively. With the exception of higher (37.2–39.5°C) lake surface apparent temperatures observed at the edge of the lake near the fumarole field, lake surface temperatures typically ranged from 21°C to 28°C (e.g. Fig. 5b). A prominent spatial pattern in lake surface temperature was evident in most TIR imagery, where a large-scale relatively cold 'plume' extended over the west side of the lake, the coolest part of which was located adjacent to the dam (Fig. 5b). In addition, narrow strands of relatively low surface temperature were observed in various parts of the lake, associated with floating mats of native sulphur.

While we can roughly compare dome fumarole and crater lake temperatures measured by the

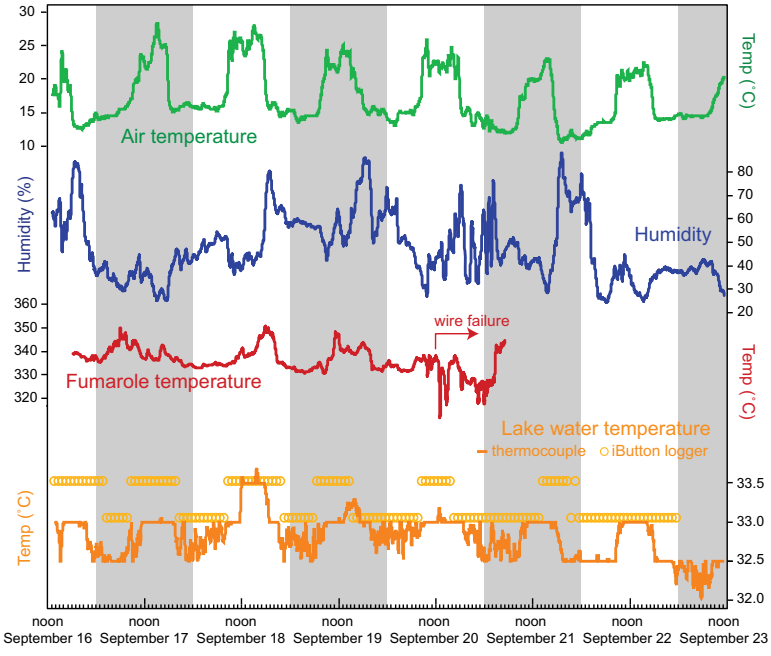

Fig. 6. Temperature and humidity logger data for thermocouple deployment at Kawah Ijen (10 min running average). Air and lake water temperatures show clear diurnal variations, which are anti-correlated with humidity. Fumarole temperatures are less systematic, but do show diurnal variability, albeit with a lag in time. The 0.5°C difference between iButton and thermocouple values is well within the accuracy of the thermocouple.

FLIR T650sc to those measured with *in situ* thermocouple and iButton methods, a direct comparison is not possible because: (1) the camera provides apparent temperatures averaged over pixels with areas larger than the footprints of the *in situ* sensors, (2) the camera provides surface apparent temperatures, whereas *in situ* measurements were made within vents or under the lake surface, and (3) we did not precisely locate the *in situ* measurements on the thermal imagery. For the dome fumaroles, a temperature of 311°C was measured by thermocouple on 15 September 2014 in vent area B, which falls within the range of apparent temperatures (up to 387°C) measured in this area using the thermal camera (Fig. 5a). Temperatures measured every 30 s by type-K thermocouple from 16 September 2014 to 23 September 2014 within vent area C varied from 330°C to 355°C, which also falls within the range of apparent temperatures (up to 382°C) measured in this area using the thermal camera (Fig. 5a). For the crater lake, temperatures measured every 60 minutes at *c.* 5 m depth by the iButton sensor (A on Fig. 5b) from 14 September 2014 to 22 September 2014 varied from *c.* 32.5°C to 33.5°C (Fig. 6), while the lake surface apparent temperature in this area was *c.* 24°C. Finally, temperatures measured every 30 s at *c.* 1.5 m depth by type-K thermocouple (B on Fig. 5b) from 16 September 2014 to 23 September 2014 were stable at around 33 $\pm$ 0.5°C (Fig. 6), whereas the lake surface apparent temperature above this site was *c.* 26°C. Taking the aforementioned sources of error into account and that additional error in camera-measured apparent temperatures can be introduced by factors such as ability to estimate emissivity, solar heating and reflection, and radiance absorption by atmospheric water vapour and SO_2 (e.g. Ball & Pinkerton 2006; Spampinato *et al.* 2011), temperatures measured using the different methods compared reasonably well.

Overall, the TIR camera provides a method for measuring apparent surface temperature at high spatial and temporal resolution over relatively large areas, while avoiding potentially hazardous conditions or loss of equipment associated with *in situ* measurements of high temperature vents and acidic lakes. We therefore recommend TIR imaging as a useful tool to monitor unrest at Kawah Ijen. In particular, installation of a permanent and automated station (e.g. Chiodini *et al.* 2007) on the crater rim should allow one to establish baseline variations in apparent temperatures, correlations between these variations, gas plume position and changes in ancillary environmental parameters, as well as

image analysis techniques to discard low-quality imagery and filter out background apparent temperature variations to better understand those variations driven by processes operating at depth in the lake and volcano.

Degassing

Multi-GAS. We conducted multi-GAS (Aiuppa *et al.* 2005; Shinohara 2005) measurements of gases emitted from the vigorously degassing fumaroles and from the crater lake at Kawah Ijen from 15–18 September 2014. Our multi-GAS included sensors for *in situ* measurements of H_2O and CO_2 (Licor 840a), SO_2 (City Technology Ltd., EZT3ST/F), and H_2S (City Technology Ltd., EZT3H) gases, plus an integrated GPS for recording position information. All data were logged at 1 Hz to a Campbell Scientific Inc. CR1000 data logger. The estimated accuracy and precision of the H_2O and CO_2 measurements are $<2\%$ and within $\sim \pm 5\%$ for SO_2 and H_2S, respectively (1σ). We operated the multi-GAS in two modes. (1) Survey measurements of the dense plume emitted from the lava dome fumaroles were made on foot on 15 September and the morning of 16 September. While in survey mode, the instrument was carried in a backpack and all data were logged continuously at 1 Hz. We present measurements from a location within the crater and about 130 m from the dome (−8.061708°, 114.244763°, 2238 m), and also from a broad saddle on the SE crater-rim (−8.063104°, 114.246200°, 2321 m) *c.* 350 m from the dome. (2) From the evening of 16 September to the morning of 18 September the instrument was temporarily deployed with an auxiliary solar-power system in a fixed location at the dam on the west side of the crater (−8.057235°, 114.237458°, 2145 m). While at the dam, the instrument automatically followed a duty cycle schedule and collected data (at 1 Hz) for a one-hour period every six hours in order to conserve power.

Fumarole plume. CO_2, SO_2 and H_2S in the vigorous plume emitted from the fumaroles were easily detected above ambient background levels during the survey measurements in the crater (Fig. 7) and from the crater rim. Water vapour was detected slightly above local background during measurements in the crater but could not be distinguished from ambient levels during measurements on the crater rim. Due to the small amount of viable water vapour data collected, the ratio of H_2O to other species should be considered poorly constrained and highly uncertain. Molar gas ratios were calculated by finding the slope of a least-square regression line fit to scatterplots of pairs of gas species (examples shown in Fig. 8). Measurements from within the crater and from the crater rim yielded equivalent results for the ratios of CO_2 and sulphur-containing gases (Fig. 8); therefore the data were pooled and used to calculate average plume gas ratios (summarized in Table 1). All of the gas species were very well correlated ($r^2 > 0.92$) with the exception of H_2O (e.g. H_2O/CO_2, $r^2 = 0.46$). The plume had a low CO_2/S_{total} ($S_{total} = SO_2 + H_2S$) ratio (2.27 ± 0.19; all ratios given as molar values and with 1σ uncertainty estimates) and SO_2 was more abundant than H_2S ($H_2S/SO_2 = 0.50 \pm 0.05$). Based on the H_2S/SO_2

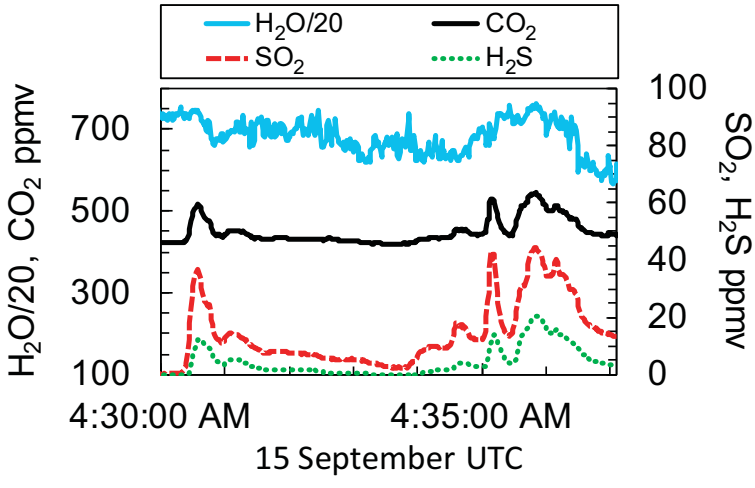

Fig. 7. Example timeseries of multi-GAS observations of the fumarole plume from within the crater ($H_2O/20$, CO_2, SO_2, H_2S).

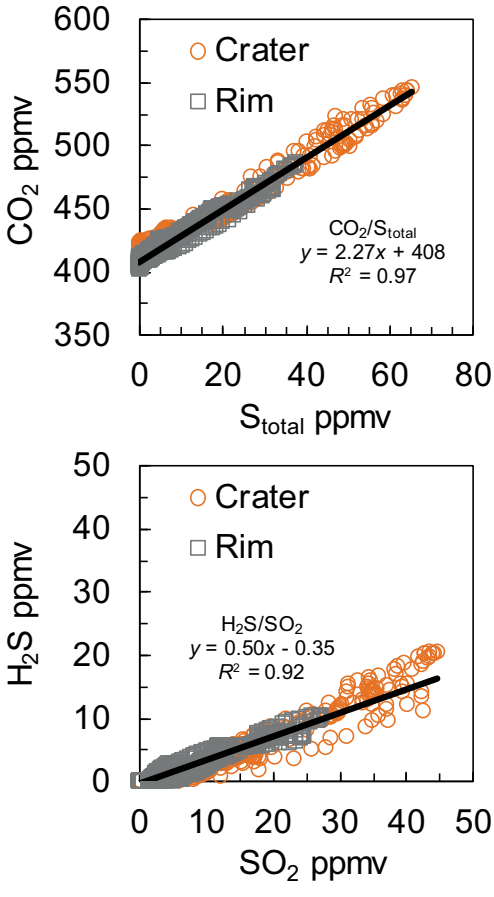

Fig. 8. Example scatterplots of multi-GAS data from the fumarole plume used to obtain gas ratios. Data were obtained from within the crater and from the crater rim.

ratio, SO_2 constituted about 67 ± 7% of total S in the plume and H_2S made up the remainder (33 ± 4%).

Our multi-GAS measurements of the plume at Kawah Ijen show some noteworthy similarities and differences when compared with direct gas samples reported by van Hinsberg *et al.* (2015) (relevant ratios are summarized in Table 1). The data reported by van Hinsberg *et al.* (2015) are from samples collected in 2007 and 2008 but represent the most recent direct samples that we are aware of. Samples have been collected by Bruce Christenson but are yet to be exported. Due to the 6–7-year gap between collection of the direct samples and the Multi-GAS observations, it is not possible to make a rigorous comparison of the two datasets. However, the available data do allow us to make speculative observations and to formulate testable hypotheses to guide future research, with the goal of developing an effective monitoring strategy at Kawah Ijen. Nevertheless, it is important to keep in mind that a priority for future research should be to collect contemporaneous direct fumarolic gas samples and Multi-GAS observations.

The most striking similarity between the direct samples and multi-GAS observations is that the CO_2/S_{total} ratios obtained by both methods are similar (direct samples $CO_2/S_{total} = 2.85 \pm 0.33$; multi-GAS $CO_2/S_{total} = 2.27 \pm 0.19$). This result suggests that the CO_2/S_{total} ratio could be monitored with a multi-GAS from the crater rim; a promising finding for gas monitoring at Kawah Ijen because one of the earliest indications of magmatic unrest at Kawah Ijen might be a pulse of CO_2-rich gas through the magma–hydrothermal system (Werner *et al.* 2011, 2012; Caudron *et al.* 2012, 2015*b*). Furthermore, it is possible to fully automate multi-GAS measurements, thereby allowing CO_2/S_{total} to be monitored in real time and without exposing personnel to hazardous conditions within the crater or during a crisis.

Despite the similarity in CO_2/S_{total} ratios from the direct samples and multi-GAS observations, the speciation of sulphur calculated by the two methods shows significant differences: sulphur in the direct samples was relatively reduced ($H_2S = 72 \pm 17\%$ of S_{total}) compared to the plume ($SO_2 = 67 \pm 7\%$ of S_{total}). The composition of the plume has changed previously (Delmelle *et al.* 2000). It is plausible that the composition of the redox state of the fumarolic sulphur changed between 2007 and 2008 and 2014, and without fumarolic data from 2014 we cannot exclude that possibility. However, given that physical characteristics of the fumarolic emissions have remained more or less constant over the period (i.e. both pressures and temperatures), we suggest a more likely explanation is that H_2S is partially combusting on contact with atmosphere, according to:

$$H_2S + 1.5O_2 \rightarrow SO_2 + H_2O \qquad (1)$$

This reaction is known to proceed along complex reaction pathways involving intermediate oxidation state S species (Merryman & Levy 1972), but the overall process is efficient at elevated temperatures in the presence of atmospheric oxygen (Frenklach *et al.* 1981). Direct evidence of this process operating at Kawah Ijen is the presence of 'blue flame' above the high temperature fumarolic emissions on the dome. As this process is somewhat temperature-dependent, however, it points to the need for both H_2S and SO_2 to be measured in the plume, and the total parameter (St) is used in conjunction with CO_2 to monitor potential changes in magmatic degassing.

Table 1. *Plume measurement using multi-GAS from the 2014 campaign and the best estimate of the gas compositions of van Hinsberg* et al. *(2015)*

	Multi-GAS (2014)			Direct samples (2007–2008)	
Fumarole gas	*mol%*	$\pm 1\sigma$	r^2	*mol%*	$\pm 1\sigma$
H_2O/CO_2	16.5	1.8	0.46	8.35	0.25
CO_2/S_{total}	2.27	0.19	0.97	2.85	0.33
CO_2/SO_2	3.42	0.26	0.96	10.2	2.7
CO_2/H_2S	6.39	0.49	0.92	3.96	0.49
H_2S/SO_2	0.501	0.050	0.92	2.57	0.75
Sulphur proportions					
$\%SO_2$	66.6%	6.9%	–	28.0%	10.7%
$\%H_2S$	33.4%	3.5%	–	72.0%	17.1%
*Lake gas**					
H_2O/CO_2	55.3	4.5	>0.80	–	–
CO_2/SO_2 (avg)	89.5	10.1	>0.90	–	–
CO_2/SO_2 (anomaly)	38.1	2.5	0.62	–	–

*no H_2S detected.
The data reported by van Hinsberg *et al.* (2015) are from samples collected in 2007 and 2008 but represent the most recent direct samples that we are aware of. The compositions of van Hinsberg *et al.* (2015) were re-normalized to a four component composition (water, CO_2, SO_2, H_2S) to compare with multi-GAS. Uncertainties of the gas ratios include the analytical uncertainties and the uncertainty in the slope of the regression line.

However, a related issue concerning S speciation and especially S emission is the interaction of the predominant volcanic S species (SO_2 and H_2S) with the enclosing hydrothermal system. The speciation behaviour of sulphur in fumarolic emissions observed during the 1995–96 eruptive period of Mt Ruapehu was found to be highly sensitive to sulphur precipitation and remobilization processes operating in the hydrothermal envelope surrounding high temperature conduits (Christenson 2000). One of the key reactions controlling S behaviour in such environments is (Mizutani & Sugiura 1966):

$$SO_2 + 2H_2S = 2H_2O + 3S \quad (2)$$

Not only is this an efficient precipitation mechanism for elemental S, but the 2:1 ratio of H_2S:SO_2 uptake from the predominant sulphur species in the volatile stream (Giggenbach 1987) can profoundly affect the speciation and overall redox state of the residual emitted gases. In the most extreme case, H_2S can be quantitatively removed from the gas stream, as demonstrated in reactive transport models from Ruapehu (Christenson *et al.* 2010).

Lake gas. H_2O, CO_2 and SO_2 were all detected during the 2.5-day long temporary deployment at the dam and the measurements show that SO_2 is being emitted directly from the surface of the hyperacidic lake at Kawah Ijen. H_2S was not detected, in agreement with the above statement on higher H_2S loss with respect to SO_2 (Tamburello *et al.* 2015). H_2O, CO_2 and SO_2 were very well correlated and from 16–18 September the 'lake gas' had an average H_2O/CO_2 ratio of 55 ± 5 and CO_2/SO_2 ratio of 90 ± 10 (Fig. 9). The CO_2/SO_2 ratio was very stable except for one notable excursion from 12:15–12:40 pm UTC on 17 September. During this time, anomalously high SO_2 values up to 3.5 ppmv were detected with a low corresponding CO_2/SO_2 ratio (38 ± 3). It is unclear if the instrument sampled gases transported from the lava dome *c.* 850 m across the lake or if excess SO_2 was periodically released from the lake. However, if 1 ppmv or more of SO_2 were transported to the dam from the fumaroles, we would expect detectable levels of H_2S, based on the H_2S/SO_2 ratio of the fumarole plume. Therefore, the possibility exists that periodic expulsions of SO_2 from the lake may occur. Interestingly, a coincident increase in seismic energy (3 minutes rolling median of the energy calculated every 20 s using the 1–10 Hz bandpass filtered waveform, Fig. 9) is observed. The variations are more pronounced for stations 1 and 4 located closer to the crater rim probably due to attenuation. Further gas and other multidisciplinary observations are needed to better put this event in context and to understand and ascertain the potential hazards posed by such a process.

In summary, we have demonstrated that Multi-GAS measurements of the bulk chemistry of the fumarole and lake plumes are a very effective monitoring tool, and that if permanently deployed, would likely greatly improve the understanding of magmatic unrest at Kawah Ijen. Longer-term measurements in one or more locations would aid

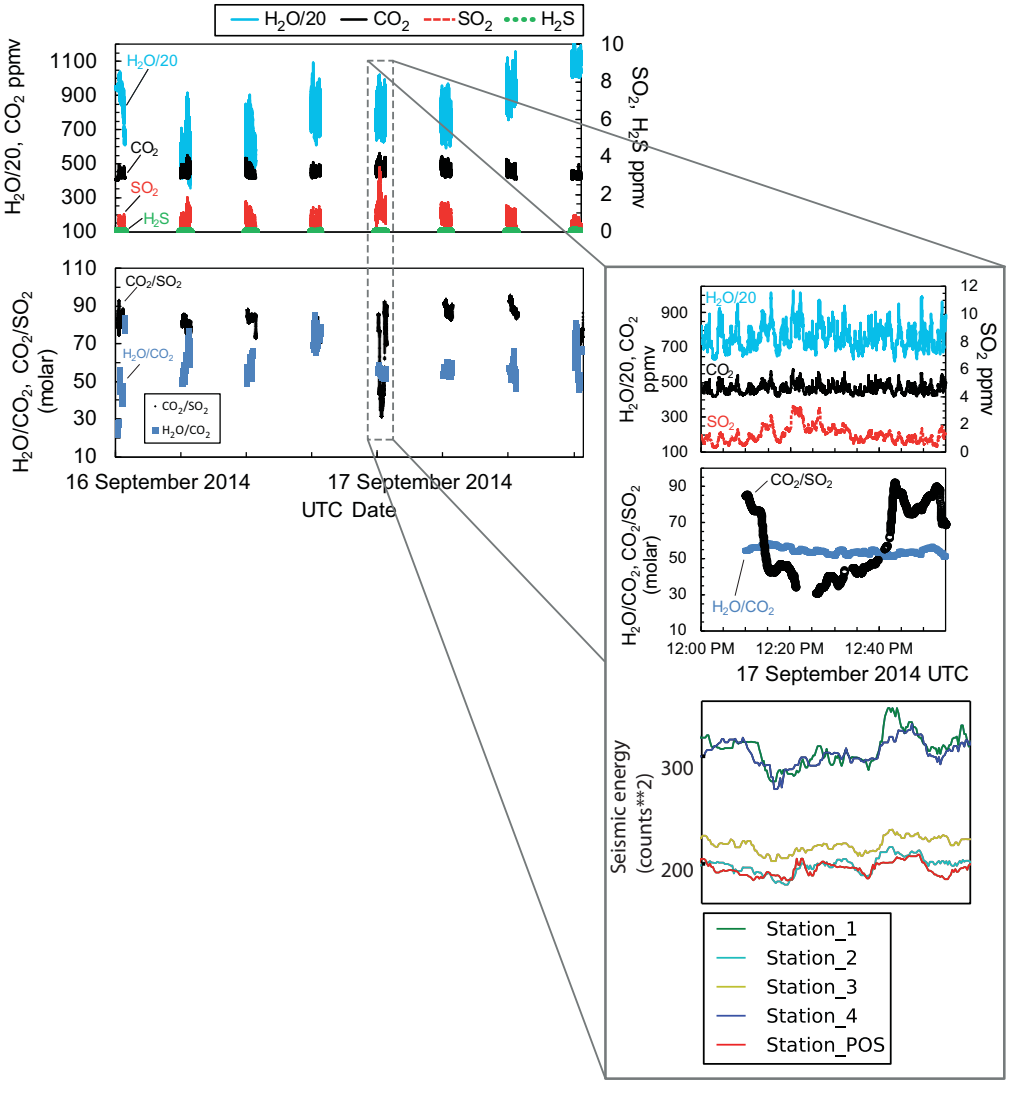

Fig. 9. Timeseries of Multi-GAS observations of 'lake gas' from a 2.5-day deployment at the dam. Ratio timeseries are 10-minute running medians filtered to include only ratios with positive slopes and an $R^2 > 0.90$. The inset figure shows the anomalously high SO_2 and change in CO_2/SO_2 ratio that was observed on 17 September. A positive correlation with seismic energies (counts squared) recorded at the array can be observed. Averages are given with 1 standard error of the mean.

in understanding the partitioning of sulphur species within the fumarole plume, between the lake fluids and lake plume, and any temporal variability coincident with shallow seismicity, which in turn would help us to understand the magmatic processes leading to changes in the superficial dynamics.

Ultraviolet SO_2 cameras. To observe the SO_2 emission from Kawah Ijen, we deployed a dual-set of Apogee Alta U260 ultraviolet cameras, on 18 September 2014 at a distance of 3 km from the source (Fig. 10a). Each camera was coupled to a Pentax B2528-UV lens, with focal length of 25 mm allowing a full angle of field-of-view (FOV) of around 24°. Immediately in front of each lens, a 10 nm full width at half maximum bandpass filter was placed: one filter was centred at 310 nm (Asahi Spectra XBPA310) where SO_2 absorbs and the other at 330 nm (XBPA330) outside the SO_2 absorption region (Mori & Burton 2006; Kantzas

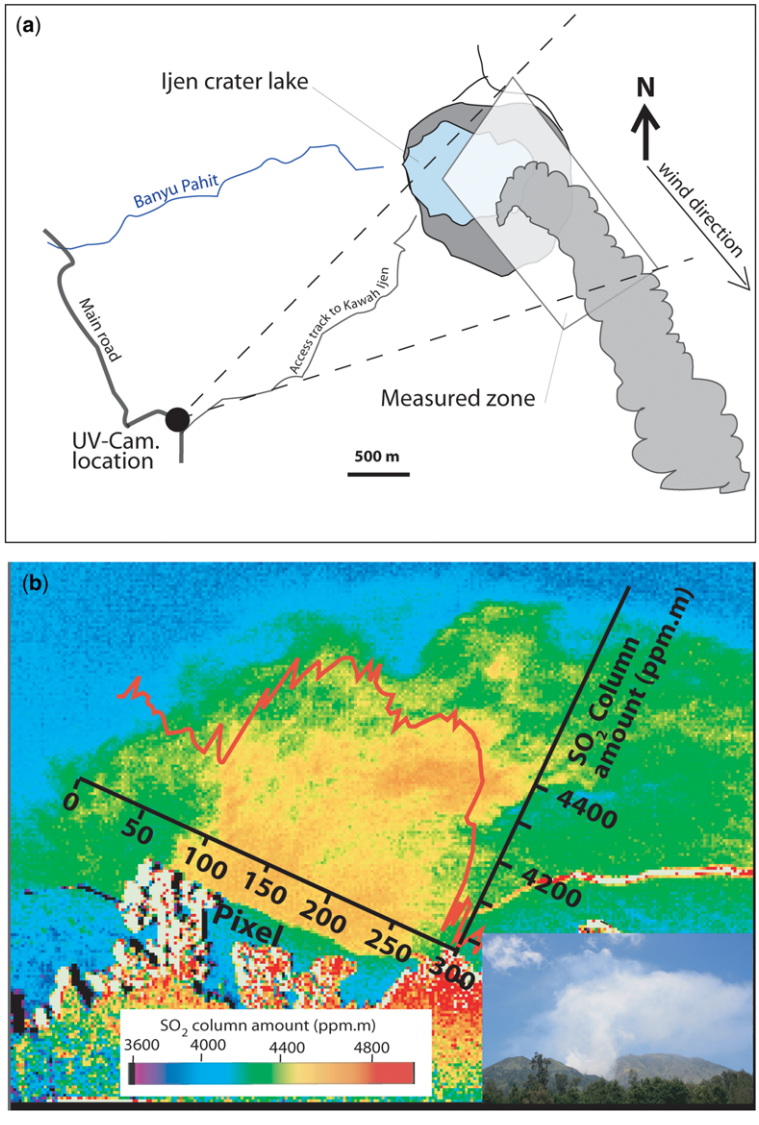

Fig 10. Sketch map of the field measurement setting (**a**) and a typical UV-cam processed image (**b**). An SO_2 column amount across the plume is highlighted by the red profile.

et al. 2010). Image acquisition and processing are achieved using Vulcamera, a stand-alone code, specifically designed for measuring volcanic SO_2 fluxes using UV cameras (Tamburello *et al.* 2011). Every image acquired is saved in a 24 bit png pixmap with a lossless compression. We used 4 SO_2 calibration cells (94, 189, 475 and 982 ppm.m) to calibrate the qualitative measured apparent absorbance (Kantzas *et al.* 2010). Two parallel sections in our data series, perpendicular to the plume transport direction, were used to derive plume speed (Tamburello *et al.* 2011). In this work we focused on the sector above the crater and the speed retrieved (5.6 m s^{-1}) rather corresponds to the plume-ascending velocity. Data were acquired from 10:46 am to 12:30 pm local time at the rate of *c.* 1 Hz. The data processing was carried out following the details outlined in Kantzas *et al.* (2010).

With nearly two hours of measurements at the acquisition rate of *c.* 1 Hz, about 6000 images are being recorded. The result of SO_2 integrated column amounts (ICA) across the plume (Fig. 11) over this recording period fluctuated between a minimum of 0.57 kg m^{-1} and maximum of 0.89 kg $m.^{-1}$ When

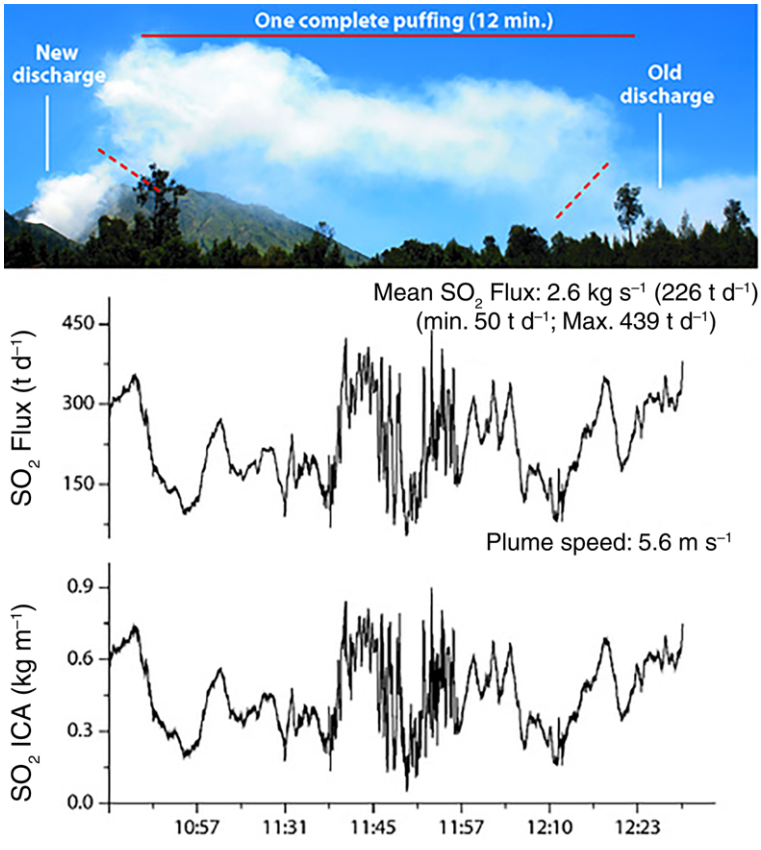

Fig. 11. SO_2 integrated column amount and SO_2 flux fluctuation recorded over the measurement period. The picture shows the puffs succession that constitutes the degassing regime of Kawah Ijen. The SO_2 peaks likely correspond to discrete puffing.

extrapolating these figures to daily estimates, the SO_2 flux over the recorded period varied between 50 and 439 t d^{-1} with a mean flux of 226 ($\pm$80) t d^{-1}, comparable to DOAS measurement results.

At least seven peaks of SO_2 flux have been observed over the approximately 2 h of continuous recordings, thus one significant increase of SO_2 flux every 10–15 mn. There is about one order of magnitude between the minimum and maximum SO_2, whilst no particular meteorological change was observed and no modifications were made in measurement settings. This periodic SO_2 flux fluctuation rather reflects the degassing regime of Kawah Ijen which appears to be sustained by periodic puffs.

DOAS. DOAS measurements were carried out at Kawah Ijen from 15–18 September 2014 to quantify the SO_2 emission rate from the lakeshore fumaroles. Evaluations were performed using the standard DOAS methodology, the details of which are described elsewhere (McGonigle *et al.* 2002; Galle *et al.* 2003; Bucsela *et al.* 2006). Varying wind directions and swirling winds within the volcano's summit crater complicated the measurements, and in many cases prohibited them altogether. The most reliable measurements were collected on 15 and 18 September.

On 15 September, winds carried the fumarolic gases to the NW and over the crater wall. To capture the emission rate, we located three DOAS instruments on the north rim of the summit crater, as shown in Figure 12. Two instruments were equipped with wide-angle optics. These were placed at a distance of 84 m from one another and pointed in parallel at the plume axis. Using a cross-correlation analysis on the time-series measured with each of these instruments (Boichu *et al.* 2010), we derived an average plume speed of 5.5 m s^{-1} in the time interval 0800–0820 UTC. The third instrument was used to scan the plume in a vertical direction, thus deriving the number of SO_2 molecules in the plume cross-section. This

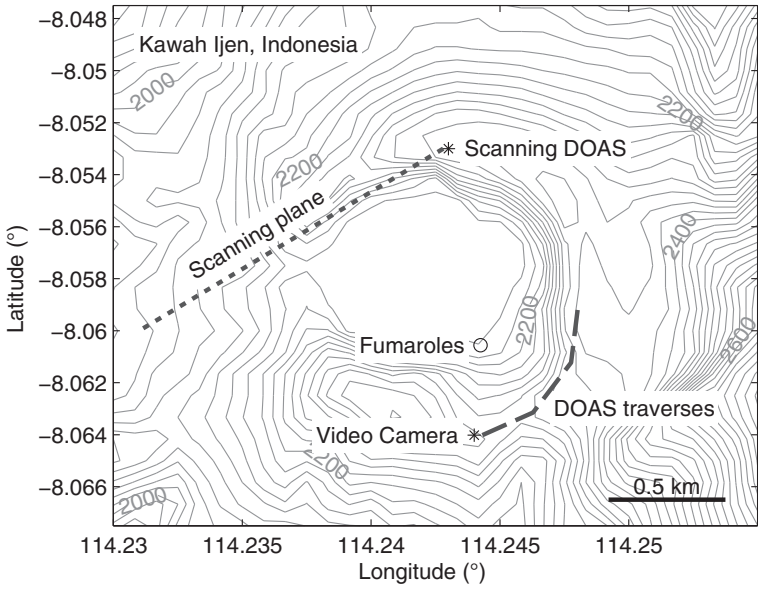

Fig. 12. Locations of the DOAS measurements performed at Kawah Ijen. On 15 September, scanning measurements were taken from the north crater rim. On 18 September, traverses were performed on the saddle on the SE crater rim. Here, the plume speed was determined by analysing video imagery taken from a fixed location on the south side of the crater.

number, multiplied by the plume speed, gives the emission rate (Galle *et al.* 2003). In the given time interval on 15 September, we derived an SO_2 emission rate of 220 ± 60 t d^{-1}.

Favourable wind conditions in the afternoon of 18 September allowed us to make walking DOAS traverse measurements on the saddle on the SE crater rim. In this geometry, a single DOAS instrument is carried beneath the gas plume in a transect that is roughly perpendicular to the plume propagation direction (McGonigle *et al.* 2002). The cross-sectional SO_2 abundance is derived by simply integrating the individual measurements. In this case, the plume speed was measured by analysing video imagery taken from a photography camera mounted on a tripod on the southern crater rim, approximately 200 m from the core of the plume. By tracking clouds of condensed steam from the left edge of the image to its right edge and timing this process, a plume speed of 3.1 m s^{-1} was obtained. When combined with the DOAS traverses, an emission rate of 155 ± 25 t d^{-1} was obtained. The derived emission rates are consistent within one standard deviation, so the difference between the derived values could be explained by the measurement uncertainty. If the uncertainties of the individual measurements are taken into account, a mean fumarolic SO_2 emission rate of about 175 t d^{-1} can be assumed.

Our SO_2 emission rates are similar to those obtained by Nathalie Vigouroux using a FLYSPEC DOAS instrument (Horton *et al.* 2006) by walking traverses. Her uncorrected SO_2 emission rates averaged for 2006–08 are 190 ± 70 t d^{-1} (van Hinsberg *et al.* 2015). This value represents a maximum estimate, because wafting of the plume over the saddle can lead to double-counting. Vigouroux-Caillibot (2011) attempted to correct for this, resulting in a minimum emission rate estimate of 25 t d^{-1} for an individual puff of gas.

Diode laser spectroscopy. A Boreal Laser Company (Edmonton, Alberta) diode laser system was deployed at Kawah Ijen. The instruments operate in the near-infrared spectral region, and emit light in narrow bandwidths coinciding with the absorption bands of target gases. Pulsed current applied to the diode cells results in small changes in cell temperature, thus changing cell dimensions and therefore the emitted wavelengths of the IR beam. This provides a 'scan' across the characteristic wavelength of the respective target gas, resulting in high-precision gas analyses.

The source and detector are co-located into a transceiver unit, from which light is propagated through the atmosphere through the target gas to a retro-reflector, and subsequently it returns to a photodiode detector in the transceiver unit

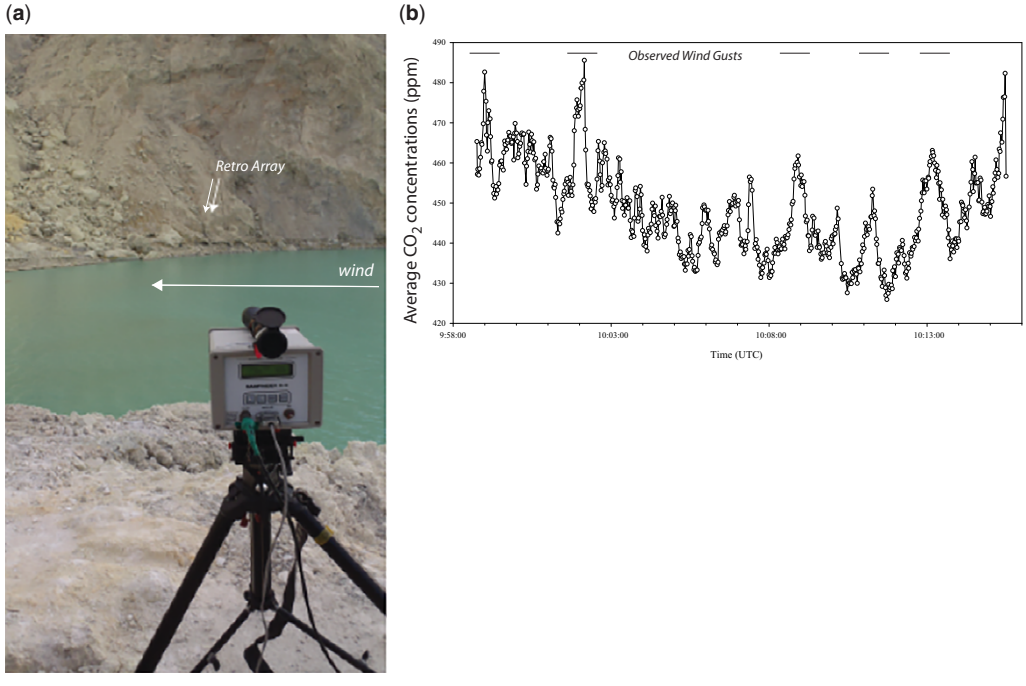

Fig. 13. CO_2 gas emissions from the lake. (**a**) location of the 97 m path measurement (Fig. 1c). (**b**) Time-series of the average CO_2 concentrations (ppm). Wind gusts are indicated with the corresponding high CO_2 concentrations.

(Fig. 13a). Absorption of the light by the target species along the pathway is quantified into average concentration along the light path according to the Beer–Lambert law.

CO_2 is usually the predominant non-condensable and inert volcanic gas released into acidic volcanic lake systems. This gas is transported from lake floor vents to the surface by buoyant convection and/or diffusional processes, from where it then diffuses across the lake surface to the atmosphere. By positioning the instrument in such a way as to achieve a beam pathway a few metres above lake level, preferably over upwellings from vents on the crater floor, we should be able to monitor the concentrations of gases coming off the lake, which will be proportional to the amount of magmatic degassing from the lake floor vents.

H_2S is another gas that is capable of being measured by this approach. Since very low levels of H_2S are emitted from the lake surface at Kawah Ijen, monitoring this gas species would allow distinction between CO_2 derived from the lake and that potentially derived from plume gas (during times of opposing wind direction(s)). This distinction should be made possible by incorporating the results of the multi-GAS results, and correcting for the fumarole component fraction.

Diode laser measurements were made for both lake water emissions and plume gases from the fumarole area. The lake surface measurements were made over a path length of 97 m on the eastern lake margin (Fig. 13a), and showed elevated values over ambient atmospheric levels (450–550 ppm v. 400 pm for atmosphere, Fig. 13b). The results also showed a strong correlation between wind speed and CO_2 concentration in the overlying air, which is related to forced convection of CO_2 across the water–atmosphere interface. This is proof of concept for the technique, which will provide insights in to lake floor venting of CO_2.

Plume measurements were made at the crater rim over a path length of 40 m. While preliminary (unprocessed) results indicate average concentrations approaching 500 ppm over the pathway, the beam was completely attenuated at times when the highest concentration plume crossed the pathway. In our opinion, the inability of the beam to penetrate the heaviest plume densities severely limits the application of this method to plume monitoring.

Since this technique operates autonomously, in real-time, it is particularly important from a health and safety standpoint during periods of unrest, when it becomes too dangerous for direct monitoring of

gas emissions by CVGHM staff. Moreover, it is not dependent on solar radiation as a light source, and hence is capable of operating 24/7.

However, it is not well-suited to conduct campaign measurements due to the significant amount of gear required. In addition to this, a power supply will be needed (solar panels and a battery bank plus protective covering situated at the transceiver end of the pathway). Additional costs include equipping the site with an ultrasonic anemometer and logger for recording wind directions, along with telemetry infrastructure. The installation and acid gas-proofing of the instrumentation is not trivial, and will require care and forethought. This technique has proven unsuitable for characterizing heavy plumes for CO_2 content (such as those at Kawah Ijen), as the high aerosol content and water condensate droplets totally absorb the beam.

High-resolution DEM

High-resolution topographic 3D point clouds are increasingly being used for detailed mapping of geological and geomorphic features of volcanic craters as well as monitoring of mass movements and deformation. Structure-from-motion photogrammetry allows the inexpensive production of 3D point clouds from collections of digital photographs, with accuracy and precision comparable to ground-based LiDAR scanning (Fonstad *et al.* 2013). We used Agisoft Photoscan Pro v1.0.4 (www.agisoft.ru) to build a 3D point cloud (Fig. 14a) and topographic model (Fig. 14b) of the Kawah Ijen crater from 1474 non-oriented photographs taken from the crater rim (Fig. 14b). We achieved basic ground control using a Garmin handheld GPS, and validated the resulting spatial reference using satellite imagery and the known location of two continuous GPS stations located along the crater rim but outside the model area. A digital elevation model (Fig. 14b) derived from the 3D point cloud (Fig. 14a) has a resolution of 0.2 m per pixel, and exhibits nearly complete spatial coverage even though portions of the crater were commonly obscured by the opaque gas plume issuing from the active fumarole. Quantitative monitoring of mass wasting and crater deformation would require installation of precisely surveyed visible benchmarks within the crater (Rouwet 2011).

Kawah Ijen conceptual model

Figure 15 presents our best estimate for a conceptual model of Kawah Ijen. A mafic magma degassing at depth supplies volatiles, metals and heat to the system, and is modified at shallow depths by interacting with a more evolved melt, likely a dacite (Berlo *et al.* 2014). These mass and heat fluxes are partially released in fumaroles from a silicic dome, and partially captured in the Kawah Ijen hydrothermal system that underlies the lake. The gradual build-up of element concentrations in this lake over time after its expulsion in 1817 suggests that

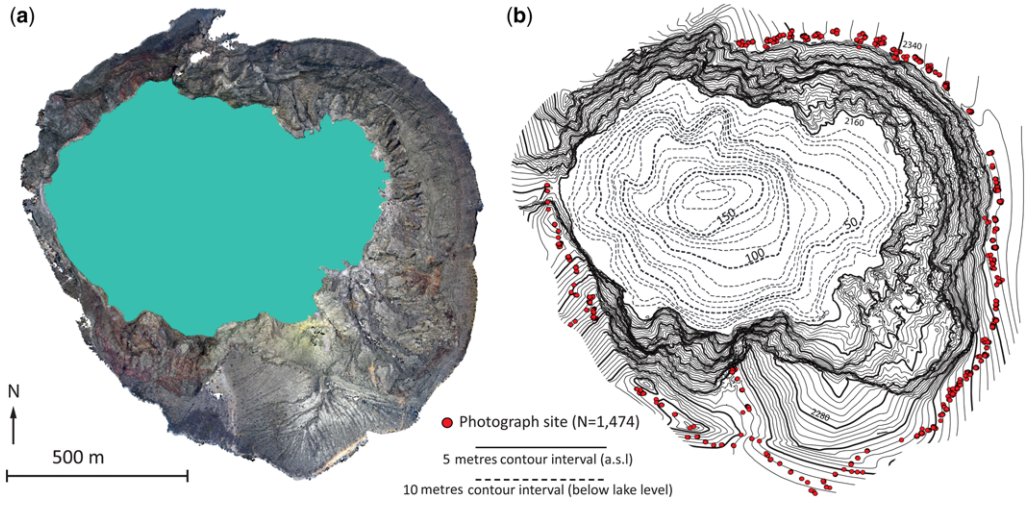

Fig. 14. Structure-from-motion topographic model of Kawah Ijen created from 1474 digital photographs (red dots) using Agisoft Photoscan. (**a**) Visualization of the 3D dense point cloud. (**b**) Contour map produced from the resulting 0.2 m resolution DEM (interval between contours is 5 m). Bathymetry is from Caudron *et al.* (2015*a*), contoured at 10 m intervals.

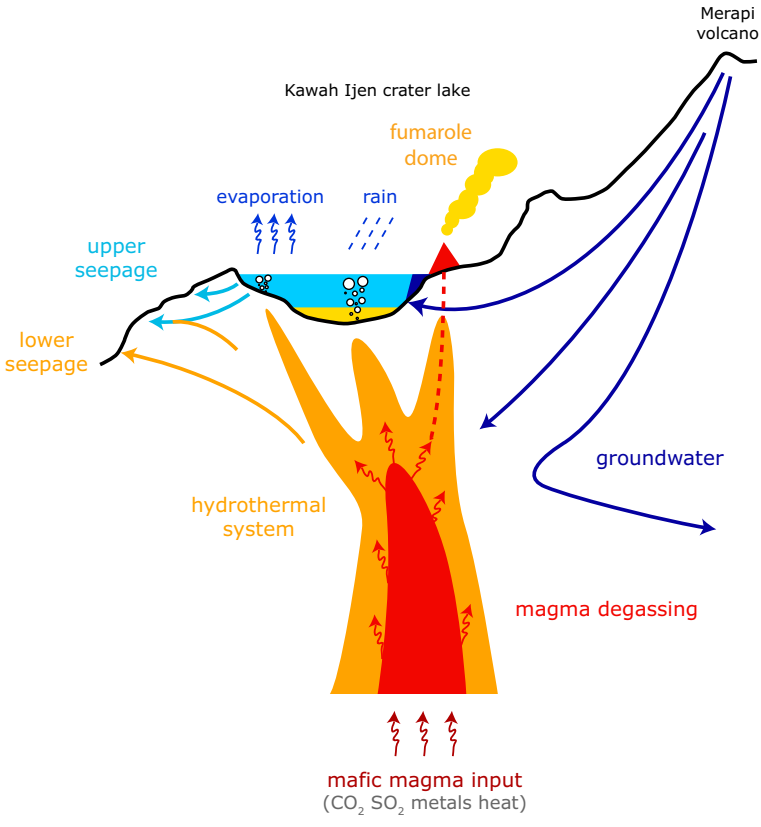

Fig. 15. Conceptual model of the Kawah Ijen system based on Palmer (2010), Berlo *et al.* (2014) and (van Hinsberg *et al.* 2015). Magmatic inputs from deep and shallow magma reservoirs combine with host-rock alteration and ground- and rainwater to form the lake, which likely hosts a native sulphur pool at depth. Seepage from the lake and hydrothermal system feeds a series of springs that form the headwaters of the Banyu Pahit River.

the hydrothermal system is not directly connected to the lake (van Hinsberg *et al.* 2015). Rather, the water budget of the lake is mainly controlled by rain and evaporation, its acidity results from volcanic gas input, and its cations are dominantly derived from leaching of wall rocks and rock fall material (Van Hinsberg *et al.* 2010*b*). Lake seepage occurs on the volcano's western flank, although the lowermost and dominant seepage area appears to have a source other than the lake on the basis of anion ratios, which Palmer *et al.* (2011) interpret to be the hydrothermal system. These seepage fluxes combine to form the acidic Banyu Pahit River. Mass balance of these fluxes indicates deposition of significant native sulphur in the lake, which agrees with older native sulphur sediments on the lake shore (Takano *et al.* 2004). Based on this conceptual model, Kawah Ijen has three main media that can be chemically monitored: (1) fumarole gas emissions; (2) lake water and its gas emissions, and; (3) acid springs and the Banyu Pahit River.

Monitoring of gas composition would thus in principle allow not only for detection of changes in the magmatic gas input, but also changes in the relative contribution of deep and shallow, or mafic and felsic magmas. Gas compositions and equilibrium temperatures (van Hinsberg *et al.* 2015) indicate that the gases reflect the volcanic vapour and thus provide a good monitoring opportunity for changes in magmatic degassing.

The lake represents a very large reservoir with high element concentrations. This means that any change in its element sources, such as an increase in volcanic gas input, will take a relatively long time before it is reflected by the lake water composition (high residence times; Rouwet *et al.* (2014*a*)). Lake water chemistry is thus not sensitive to short-term changes in the state of the system and is not an effective monitoring media. However, non-condensable gases such as CO_2 are almost completely transmitted through the lake and should therefore directly reflect changes in volcanic

gas input at depth, and provide a good monitoring opportunity.

There are three main areas of acid seepage on the west and SW flank of Kawah Ijen. Of these, the lowermost one has by far the highest discharge and dominates input into the acidic Banyu Pahit River. We interpret this spring as emitting waters derived from the underlying hydrothermal system (Palmer 2010), and its composition should thus be sensitive to changes in the deep magmatic–hydrothermal system. Water composition shows no significant change from the springs to the waterfall at Watu Capil (Van Hinsberg *et al.* 2010*b*), allowing easy access to these waters for sampling. The upstream Banyu Pahit River therefore provides a good opportunity to monitor the magmatic–hydrothermal system and any changes in its input, and is a more sensitive and hence better monitoring medium than the lake.

Conclusions

A unique workshop took place at Kawah Ijen volcano from 14–21 September 2014. Twenty-five participants (from 10 countries) deployed a wide variety of geophysical and geochemical instruments and sampling equipment on the volcano, tested techniques and determined their feasibility for the future CVGHM monitoring programme. Discussions of techniques and results, a half-day field trip through parts of the Kawah Ijen caldera, and multinational installation and data processing teams stimulated productive exchanges, cross-training and technology transfer. Presentations and discussions by participants from different countries highlighted analogous volcanoes, monitoring data utilized, techniques and 'tricks of the trade', as well as interpretations of the magmatic and hydrothermal processes that give rise to the monitoring signals that are important in forecasting at wet volcanoes. One particularly relevant example was the identification of Ruapehu volcano, New Zealand, as a 'sister volcano' of Kawah Ijen, with remarkably similar geological structures and well-studied geochemical/geophysical processes. In the absence of modern historical (i.e. monitored) eruptions at a wet volcano, data from analogous volcanoes such as Ruapehu may aid in interpretation and identification of precursory signals prior to eruptive events. Relationships such as these highlight the importance of data dissemination via freely available global platforms such as WOVOdat (reference).

Dmitri Rouwet was funded by EC Framework Program 7 under grant agreement number 282759: 'VUELCO'. Vincent van Hinsberg and Sri Budhi Utami acknowledge financial support from NSERC, the Mineralogical Association of Canada and Osisko.

References

Aiuppa, A., Federico, C., Giudice, G. & Gurrieri, S. 2005. Chemical mapping of a fumarolic field: la Fossa crater, Vulcano Island (Aeolian Islands, Italy). *Geophysical Research Letters*, **32**, L13309

Arrowsmith, S.J., Johnson, J.B., Drob, D.P. & Hedlin, M.A. 2010. The seismoacoustic wavefield: a new paradigm in studying geophysical phenomena. *Reviews of Geophysics*, **48**, RG4003.

Ball, M. & Pinkerton, H. 2006. Factors affecting the accuracy of thermal imaging cameras in volcanology. *Journal of Geophysical Research: Solid Earth (1978–2012)*, **111**, B11203.

Berlo, K., van Hinsberg, V.J., Vigouroux, N., Gagnon, J.E. & Williams-Jones, A.E. 2014. Sulfide breakdown controls metal signature in volcanic gas at Kawah Ijen volcano, Indonesia. *Chemical Geology*, **371**, 115–127, http://doi.org/10.1016/j.chemgeo.2014.02.009

Boichu, M., Oppenheimer, C., Tsanev, V. & Kyle, P.R. 2010. High temporal resolution SO_2 flux measurements at Erebus volcano, Antarctica. *Journal of Volcanology and Geothermal Research*, **190**, 325–336.

Bosch, C.J. 1858. Uitbarstingen der vulkanen Idjin en Raun (Banjoewangi). *In*: *Tijdschrift voor Indische Taal-, Land- en Volkenkunde*, **7**, 265–286

Bucsela, E.J., Celarier, E.A., Wenig, M.O., Gleason, J.F., Veefkind, J.P., Boersma, K.F. & Brinksma, E.J. 2006. Algorithm for no 2 vertical column retrieval from the ozone monitoring instrument. *IEEE Transactions on Geoscience and Remote Sensing*, **44**, 1245–1258.

Caudron, C., Mazot, A. & Bernard, A. 2012. Carbon dioxide dynamics in Kelud volcanic lake. *Journal of Geophysical Research: Solid Earth*, **117**, B05102.

Caudron, C., Syahbana, D.K. *et al.* 2015*a*. Kawah Ijen volcanic activity: a review. *Bulletin of Volcanology*, **77**, 1–39.

Caudron, C., Lecocq, T. *et al.* 2015*b*. Stress and mass changes at a 'wet' volcano: Example during the 2011–2012 volcanic unrest at Kawah Ijen volcano (Indonesia). *Journal of Geophysical Research: Solid Earth*, **120**, 5117–5134, http://doi.org/10.1002/2014JB011590

Chiodini, G., Vilardo, G., Augusti, V., Granieri, D., Caliro, S., Minopoli, C. & Terranova, C. 2007. Thermal monitoring of hydrothermal activity by permanent infrared automatic stations: results obtained at Solfatara di Pozzuoli, Campi Flegrei (Italy). *Journal of Geophysical Research: Solid Earth (1978–2012)*, **112**, B12206.

Christenson, B. 2000. Geochemistry of fluids associated with the 1995–1996 eruption of Mt. Ruapehu, New Zealand: signatures and processes in the magmatic-hydrothermal system. *Journal of Volcanology and Geothermal Research*, **97**, 1–30.

Christenson, B., Reyes, A., Young, R., Moebis, A., Sherburn, S., Cole-Baker, J. & Britten, K. 2010. Cyclic processes and factors leading to phreatic eruption events: insights from the 25 September 2007 eruption through Ruapehu Crater Lake, New Zealand. *Journal of Volcanology and Geothermal*

Research, **191**, 15–32, http://doi.org/10.1016/j.jvolgeores.2010.01.008

Delmelle, P. & Bernard, A. 1994. Geochemistry, mineralogy, and chemical modeling of the acid crater lake of Kawah Ijen Volcano, Indonesia. *Geochimica et Cosmochimica Acta*, **58**, 2445–2460

Delmelle, P., Bernard, A., Kusakabe, M., Fischer, T.P. & Takano, B. 2000. Geochemistry of the magmatic-hydrothermal system of Kawah Ijen volcano, East Java, Indonesia. *Journal of Volcanology and Geothermal Research*, **97**, 31–53.

Endo, E.T. & Murray, T. 1991. Real-time seismic amplitude measurement (RSAM): a volcano monitoring and prediction tool. *Bulletin of Volcanology*, **53**, 533–545, http://doi.org/10.1007/BF00298154

Fonstad, M.A., Dietrich, J.T., Courville, B.C., Jensen, J.L. & Carbonneau, P.E. 2013. Topographic structure from motion: a new development in photogrammetric measurement. *Earth Surface Processes and Landforms*, **38**, 421–430.

Frenklach, M., Lee, J., White, J. & Gardiner, W.J. 1981. Oxidation of hydrogen sulfide. *Combustion and Flame*, **41**, 1–16.

Galle, B., Oppenheimer, C., Geyer, A., McGonigle, A.J., Edmonds, M. & Horrocks, L. 2003. A miniaturised ultraviolet spectrometer for remote sensing of SO_2 fluxes: a new tool for volcano surveillance. *Journal of Volcanology and Geothermal Research*, **119**, 241–254.

Giggenbach, W. 1987. Redox processes governing the chemistry of fumarolic gas discharges from White Island, New Zealand. *Applied Geochemistry*, **2**, 143–161.

Gunawan, H., Pallister, J. & Caudron, C. 2014. Multidisciplinary Monitoring Experiments at Kawah Ijen Volcano. *Eos, Transactions American Geophysical Union*, **95**, 447–448.

Handley, H.K., Macpherson, C.G., Davidson, J.P., Berlo, K. & Lowry, D. 2007. Constraining fluid and sediment contributions to subduction-related magmatism in Indonesia: Ijen Volcanic Complex. *Journal of Petrology*, **48**, 1155–1183.

Horton, K.A., Williams-Jones, G. *et al.* 2006. Real-time measurement of volcanic SO_2 emissions: validation of a new UV correlation spectrometer (FLYSPEC). *Bulletin of Volcanology*, **68**, 323–327.

Johnson, J.B. & Ripepe, M. 2011. Volcano infrasound: a review. *Journal of Volcanology and Geothermal Research*, **206**, 61–69.

Johnson, J.B. & Ronan, T.J. 2015. Infrasound from volcanic rockfalls. *Journal of Geophysical Research: Solid Earth*, **120**, 8223–8239.

Jolly, A., Sherburn, S., Jousset, P. & Kilgour, G. 2010. Eruption source processes derived from seismic and acoustic observations of the 25 September 2007 Ruapehu eruption – North Island, New Zealand. *Journal of Volcanology and Geothermal Research*, **191**, 33–45.

Jones, K. & Johnson, J. 2011. Mapping complex vent eruptive activity at Santiaguito, Guatemala using network infrasound semblance. *Journal of Volcanology and Geothermal Research*, **199**, 15–24.

Kantzas, E.P., McGonigle, A., Tamburello, G., Aiuppa, A. & Bryant, R.G. 2010. Protocols for UV camera volcanic SO_2 measurements. *Journal of Volcanology and Geothermal Research*, **194**, 55–60.

Kilgour, G., Saunders, K., Blundy, J., Cashman, K., Scott, B. & Miller, C. 2014. Timescales of magmatic processes at Ruapehu volcano from diffusion chronometry and their comparison to monitoring data. *Journal of Volcanology and Geothermal Research*, **288**, 62–75.

Löhr, A., Bogaard, T. *et al.* 2005. Natural pollution caused by the extremely acid crater lake Kawah Ijen, East Java, Indonesia. *Environmental Science and Pollution Research*, **12**, 89–95.

Manville, V. 2015. Volcano-hydrologic hazards from volcanic lakes. *In*: *Volcanic Lakes*, Springer, Berlin, 21–71.

McGonigle, A., Oppenheimer, C., Galle, B., Mather, T. & Pyle, D. 2002. Walking traverse and scanning doas measurements of volcanic gas emission rates. *Geophysical Research Letters*, **29**, 46–41.

Merryman, E.L. & Levy, A. 1972. Disulfur and the lower oxides of sulfur in hydrogen sulfide flames. *The Journal of Physical Chemistry*, **76**, 1925–1931.

Mizutani, Y. & Sugiura, T. 1966. The chemical equilibrium of the $2H_2S + SO_2 = 3S + 2H_2O$ reaction in Solfataras of the Nasudake Volcano. *Bulletin of the Chemical Society of Japan*, **39**, 2411–2414.

Mori, T. & Burton, M. 2006. The SO_2 camera: a simple, fast and cheap method for ground-based imaging of SO_2 in volcanic plumes. *Geophysical Research Letters*, **33**, L24804.

Nairn, I., Wood, C. & Hewson, C. 1979. Phreatic eruptions of Ruapehu: April 1975. *New Zealand Journal of Geology and Geophysics*, **22**, 155–170.

Palmer, S. 2010. *Hydrogeochemistry of the upper Banyu Pahit River valley, Kawah Ijen volcano, Indonesia*. Master's thesis, McGill University.

Palmer, S.J., van Hinsberg, V.J., McKenzie, J.M. & Yee, S. 2011. Characterization of acid river dilution and associated trace element behavior through hydrogeochemical modeling: a case study of the Banyu Pahit River in East Java, Indonesia. *Applied Geochemistry*, **26**, 1802–1810.

Ripepe, M., Marchetti, E. & Ulivieri, G. 2007. Infrasonic monitoring at Stromboli volcano during the 2003 effusive eruption: insights on the explosive and degassing process of an open conduit system. *Journal of Geophysical Research: Solid Earth*, **112**, B09207.

Rouwet, D. 2011. A photographic method for detailing the morphology of the floor of a dynamic crater lake: the El Chichón case (Chiapas, Mexico). *Limnology*, **12**, 225–233.

Rouwet, D., Tassi, F., Mora-Amador, R., Sandri, L. & Chiarini, V. 2014*a*. Past, present and future of volcanic lake monitoring. *Journal of Volcanology and Geothermal Research*, **272**, 78–97.

Rouwet, D., Sandri, L., Marzocchi, W., Gottsmann, J., Selva, J., Tonini, R. & Papale, P. 2014*b*. Recognizing and tracking volcanic hazards related to non-magmatic unrest: a review. *Journal of Applied Volcanology*, **3**, 1–17.

Shinohara, H. 2005. A new technique to estimate volcanic gas composition: plume measurements with a

portable multi-sensor system. *Journal of Volcanology and Geothermal Research*, **143**, 319–333.

SPAMPINATO, L., CALVARI, S., OPPENHEIMER, C. & BOSCHI, E. 2011. Volcano surveillance using infrared cameras. *Earth-Science Reviews*, **106**, 63–91.

TAKANO, B., SUZUKI, K. *ET AL*. 2004. Bathymetric and geochemical investigation of Kawah Ijen crater lake, East Java, Indonesia. *Journal of Volcanology and Geothermal Research*, **135**, 299–329.

TAMBURELLO, G., KANTZAS, E.P., MCGONIGLE, A.J. & AIUPPA, A. 2011. Vulcamera: a program for measuring volcanic SO_2 using UV cameras. *Annals of Geophysics*, **54**, 219–221.

TAMBURELLO, G., AGUSTO, M. *ET AL*. 2015. Intense magmatic degassing through the lake of Copahue volcano, 2013–2014. *Journal of Geophysical Research: Solid Earth*, **120**, 6071–6084.

UTAMI, S. 2015. *Gypsum as a recorder of fluid chemistry and temperature at Kawah Ijen volcano, East Java, Indonesia*. Master's thesis, McGill University.

VAN HINSBERG, V., BERLO, K., VAN BERGEN, M. & WILLIAMS-JONES, A. 2010*a*. Extreme alteration by hyperacidic brines at Kawah Ijen volcano, East Java, Indonesia: I. Textural and mineralogical imprint. *Journal of Volcanology and Geothermal Research*, **198**, 253–263, http://doi.org/10.1016/j.jvolgeores.2010.09.002

VAN HINSBERG, V., BERLO, K., SUMARTI, S., VAN BERGEN, M. & WILLIAMS-JONES, A. 2010*b*. Extreme alteration by hyperacidic brines at Kawah Ijen volcano, East Java, Indonesia: II. Metasomatic imprint and element fluxes. *Journal of Volcanology and Geothermal Research*, **196**, 169–184.

VAN HINSBERG, V., VIGOUROUX, N. *ET AL*. 2015. Element flux to the environment of the passively degassing crater lake-hosting Kawah Ijen volcano, Indonesia, and implications for estimates of the global volcanic flux. *In*: OHBA, T., CAPACCIONI, B. & CAUDRON, C. (eds) *Geochemistry and Geophysics of Active Volcanic Lakes*. Geological Society, London, Special Publications, **437**. First published online December 12, 2015, http://doi.org/10.1144/SP437.2

VIGOUROUX-CAILLIBOT, N. 2011. *Tracking the evolution of magmatic volatiles from the mantle to the atmosphere using integrative geochemical and geophysical methods*. PhD thesis, Department of Earth Sciences-Simon Fraser University.

WERNER, C., EVANS, W.C., KELLY, P.J., MCGIMSEY, R., PFEFFER, M., DOUKAS, M. & NEAL, C. 2012. Deep magmatic degassing v. scrubbing: elevated CO_2 emissions and C/S in the lead-up to the 2009 eruption of Redoubt Volcano, Alaska. *Geochemistry, Geophysics, Geosystems*, **13** Q0301.

WERNER, C.A., DOUKAS, M.P. & KELLY, P.J. 2011. Gas emissions from failed and actual eruptions from Cook Inlet Volcanoes, Alaska, 1989–2006. *Bulletin of Volcanology*, **73**, 155–173.